Molecular characterization of copper-dependent enzymes involved in Streptomyces morphology

Petrus, Maria Louise Catharina

4

Abstract

Streptomyces lividans displays a distinct dependence on copper to fully initiate morphological development. Evidence has accumulated to implicate the participation of an extracytoplasmic cuproenzyme in morphogenesis. Here we show that GlxA is this cuproenzyme. GlxA is membrane associated and has an active site consisting of a mononuclear copper and a cross-linked Tyr-Cys co-factor. The domain organisation of the tertiary structure defines GlxA as a new structural member of the mono-copper oxidase family, with copper coordination geometry similar to, but spectroscopically distinct from fungal galactose oxidase. Electron paramagnetic resonance spectroscopy reveals that the oxidation of cupric GlxA generates a protein radical residing on the Tyr-Cys cross-link. A variety of canonical galactose oxidase substrates (including D-galactose) were tested but none were readily turned over by GlxA. A *glxA* null-mutant leads to loss of glycan accumulation at hyphal tips and consequently a drastically changed morphology both on solid substrates and in liquid-grown environments, a scenario similarly observed in the absence of the neighbouring glycan synthase CslA. The *glxA* mutant phenotype cannot be rescued by addition of copper suggesting it is the enzymatic action of GlxA on the glycan that is required for development and morphology. From a biotechnology perspective the open mycelium morphology observed with the *glxA* mutant in submerged culture has implications for use as an enzyme production host.

This Chapter was published as:

Amanda K. Chaplin, Marloes L.C. Petrus, Giulia Mangiameli, Michael A. Hough, Dimitri A. Svistunenko, Peter Nicholls, Dennis Claessen, Erik Vijgenboom and Jonathan A.R. Worrall (2015). Biochemical Journal 469: 433-444

GlxA is a new structural member of the radical copper oxidase family and is required for glycan deposition at hyphal tips and morphogenesis of *Streptomyces lividans*

Introduction

Streptomycetes are filamentous monoderm soil bacteria that form networks of branching hyphae called mycelia. These organisms display a complex developmental life cycle on solid substrates. Following spore germination a vegetative mycelium is established that in response to nutrient depletion and other signals initiates both secondary metabolite production and morphological differentiation (Flärdh and Buttner, 2009; van Dissel *et al.*, 2014). This leads to the formation of aerial hyphae that will develop into chains of spores. The richness and varied production of secondary metabolites in streptomycetes is coordinated with development and these metabolites have long been a source of interest due to their pharmaceutical properties (Flärdh and Buttner, 2009; van Dissel *et al.*, 2014). Streptomycetes also hold promise as a large scale production host in biotechnology for the heterologous production of proteins and enzymes at high levels for therapeutic, scientific, diagnostic and agricultural purpose (Anné *et al.*, 2012). *Streptomyces lividans* is a preferred choice as an industrial host primarily due to its low level of endogenous extracellular proteolytic activity. As a production host the morphology of the mycelial growth in submerged culture is important as this can play a significant role in its production capacity (van Dissel et al., 2014).

Copper (Cu) is an essential redox-active metal ion in living organisms. In *S. lividans* a distinct dependence on the bioavailability of Cu in order to fully initiate morphological development is known (Keijser *et al.*, 2000; Fujimoto *et al.*, 2012; Blundell *et al.*, 2013). *In vitro* studies have revealed that two extracytoplasmic Cu metallochaperones, ECuC and Sco, facilitate a Cu trafficking pathway whereby the Sco protein can receive Cu from ECuC and deliver it to the Cu_A site of an aa_3-type cytochrome *c* oxidase (CcO). Mutant analysis in *S. lividans* has revealed that morphological development proceeds in the absence of ECuC (Δ*ecuc*) and CcO

(Δ*cco*), but not in the absence of Sco (Δ*sco*). While Δ*ecuc* and Δ*sco* significantly reduce CcO activity, these data indicate that morphological development is not linked to impaired CcO activity (Blundell *et al.*, 2013). Notably the addition of exogenous Cu to the Δ*sco* mutant rescues development (Blundell *et al.*, 2013). This implies that a branched Cu trafficking pathway is prevalent under Cu homeostasis conditions in *S. lividans*, whereby Sco is most certainly required to act as a Cu chaperone for CcO and possibly for other extracytoplasmic cupro-proteins/enzymes that trigger formation of aerial hyphae (Blundell *et al.*, 2014).

Analysis of the *S. lividans* genome has revealed a number of genes that encode for putative extracytoplasmic cuproenzymes (Worrall and Vijgenboom, 2010; Cruz-Morales *et al.*, 2013). One of these, SLI_3188, has a weak sequence homology with the secreted fungal cuproenzyme galactose oxidase (Gox), with putative ligands to the Cu ion (two Tyr and two His residues) seemingly conserved (Supplementary Fig. S1). Gox houses a catalytic unit, which combines two distinct redox centres; a mononuclear Cu site capable of one electron redox cycling and a Tyr-Cys cofactor, whereby a Cys residue is cross-linked to one of the Cu coordinating Tyr residue and can form a stable protein radical (Whittaker and Whittaker, 1988; Whittaker and Whittaker, 1990; Ito *et al.*, 1991; Whittaker and Whittaker, 1993; Ito *et al.*, 1994; Lee *et al.*, 2008). This redox unit enables the two-electron oxidation of a range of D-isomers of primary alcohols (including the C6-hydroxylmethyl group of mono- and polysaccharides) to aldehydes with the reduction of dioxygen to hydrogen peroxide (Avigad *et al.*, 1962). The physiological function of Gox remains unknown, but the broad substrate specificity inherent in this cuproenzyme suggests that maintaining hydrogen peroxide production in the extracytoplasmic environment may be important for function.

In *S. coelicolor* a homologous gene to *SLI_3188*, annotated as *glxA*, is required for aerial hyphae development under conditions of osmotic stress (Liman *et al.*, 2013). The *glxA* gene is the distal gene in an operon with *cslA*, which encodes a family 2 glycosyltransferase that synthesizes a glycan at hyphal tips (Xu *et al.*, 2008; Petrus and Claessen, 2014). Orthologs of *glxA* and *cslA* are present in all streptomycetes and several other actinobacteria with some species having paralogs e.g. *S. griseus* and *S. albus*. The genetic locus contains several other genes encoding enzymes implicated in glycan processing, including a Cu-containing lytic polysaccharide monooxygenase, suggesting a role of GlxA in polysaccharide modification or synthesis. In the present study we show that GlxA is a membrane-associated cuproenzyme with a mononuclear Cu site and a Tyr-Cys redox cofactor. However, GlxA is distinct from fungal Gox through a unique tertiary structure, atypical spectroscopic properties, and a lack of enzymatic activity with a range of 'classical' Gox substrates. As observed in the absence of *cslA*, we find that a *glxA* null-mutant stalls aerial hyphae development on solid media, lacks the hyphal tip glycan and has a dramatically different morphology in liquid-grown cultures. The latter is of particular interest in respect to the use of *S. lividans* as a cell factory for protein production.

Experimental

Mycelium washes, fractionation and GlxA detection

S. lividans 1326 was grown in TSBS for 18 h at 30 °C with shaking at 200 rpm. Mycelium was harvested in 1.5 ml aliquots by centrifugation at 15,000 g for 10 min and stored at -80 °C until required. Mycelium aliquots were first resuspended in 25 mM Tris/HCl pH 7.5, 100 mM NaCl centrifuged at 25,000 g and the supernatant was kept as the 100 mM NaCl wash. The pellet was resuspended in buffer containing 1 M NaCl, incubated for 30 min on ice and centrifuged at 25,000 g, which produced the 1 M NaCl wash. For mycelium extracts the suspended mycelium pellets were sonicated (Bioruptor, 12 cycles 30 s on, 30 s off). The soluble (S30) and insoluble fractions (P30) were obtained by centrifugation at 30,000 g. The supernatant (S30) was subjected to a second centrifugation step at 100,000 g to remove all membrane particles and ribosomes to give the S100 and P100 fractions. The pellets (P30 and P100) was resuspended in buffer containing 1 % Triton X-100, incubated on ice for 30 min and centrifuged again at 30,000 g and 100,000 g, respectively to separate triton soluble (P30-TS, P100-TS) and insoluble (P30-TP, P100-TP) fractions. Fractions obtained were run on 10 % SDS-PAGE and blotted to Hybond-P membranes for immuno-detection of GlxA and EF-Tu1. The antibodies against GlxA were a kind gift of James W. Whittaker (Oregon Health & Science University, USA). The EF-Tu1 antibodies were raised in rabbits against *S. ramocissimus* EF-Tu1 (Vijgenboom *et al.*, 1994). Incubation with antibodies (GlxA antibodies 10,000 x diluted and EF-Tu1 antibodies 5,000 x diluted) was carried out for 18 h at 4 °C with gentle rocking in PBS with 5 % milk (FrisoLac Extra, FrieslandCampina). The bound antibodies were detected with GARAP (Sigma) as the secondary antibody and NBT/BCIP as the substrate. Digital images were taken of the Western blots and total signal intensities were determined with Image J (Schneider *et al.*, 2012).

Creation of the S. lividans ΔcslA and ΔglxA null-mutants, complementation plasmids and monitoring growth morphology

The Δ*glxA* and Δ*cslA* mutant was prepared and isolated as previously described (Blundell *et al.*, 2013). In the Δ*glxA* mutant, nucleotides +60 to +1916 relative to the start codon of *SLI_3188* were replaced by a 62 nt scar of the *loxP* recombination site including two *Xba*I sites. In the Δ*cslA* mutant, nucleotides +79 to +1827 relative to the start of *SLI_3187* were replaced. The mutant is consistent with the one described by Xu *et al.* (2008). Plasmid pGlxA contains the *glxA* ORF (SLI_3188) and the promoter region (-545 to -1) upstream of *cslA* (SLI_3187). For surface growth the agar media R5 (Kieser *et al.*, 2000) was incubated at 30 °C, and supplemented with Cu as required. Morphology in liquid media was determined following 24 h growth at 30 °C with shaking in flasks equipped with coils containing Tryptic

Soya Broth (TSB) supplemented with 10 % sucrose and Cu as indicated. Samples from liquid cultures were analysed by light microscopy with a Zeiss Standard 25 microscope and digital pictures were taken with an AxioCam camera linked to AxioVision software. All spore stocks were obtained from cultures grown on MS agar plates (Kieser *et al.*, 2000) and stored in 20 % glycerol at -20 ^{o}C.

Monitoring glycan production

Glycan production was determined following 24 h growth at 30 ºC in 8 well microscopy plates (Lab-TEK II Chambered Coverglass) containing 500µl mNMMP medium [24]. Mycelium was stained by adding 50 µl calcofluor white (CFW) solution (Remel Bactidrop) to each well. After 5min, but within 20 min, stained mycelium was analysed with a laser-scanning confocal microscope (Zeiss LSM5 Exciter/Axio Observer) by excitation with a 405 nm laser, a 405/488 nm beamsplitter and a bandpass emission filter of 420-480 nm. Images were adjusted for brightness and contrast using ImageJ (Schneider et al., 2012).

Cloning, over-expression and purification of GlxA

The *glxA* gene with 200 flanking nt at the 5' and 3' ends was amplified from *S. lividans* 1326 and cloned into a pUC19 vector. This construct was used to create an N-terminal deleted *glxA* for over-expression in *Escherichia coli* by amplifying the *glxA* nt sequence that starts coding for amino acid 35, and restricted using the *Nde*I and *Bam*HI sites of a pET28a vector (Novagen) to create an N-terminal His_6-tagged *glxA* construct. The overexpression and purification of recombinant GlxA are described in Supporting Information.

Preparation of GlxA samples and UV-visible spectroscopy

GlxA concentration was determined by UV-visible spectroscopy (Varian Cary 50 UV-visible spectrophotometer) using an extinction coefficient (ε) at 280 nm of 78,730 $M^{-1}\cdot cm^{-1}$. The various forms of GlxA were prepared through the addition of ~ 5-fold excess of $[Fe(CN)_6]^{3-}$ (Sigma), $[Ir(Cl)_6]^{3-}$ (Acros) or $Na_2S_2O_4$ (Sigma) followed by removal via a PD-10 column (GE Healthcare).

Crystallisation and structure determination

An ARI-Gryphon 96-well crystallisation robot was used to screen crystallisation conditions for GlxA. A crystal hit was discovered in 0.1 M sodium acetate pH 4.6, 15% PEG 20,000 (PEG suite, Qiagen). Scaling-up and optimisation of GlxA crystals from the initial hit was carried out in 24-well VDX plates (Molecular Dimensions) using the hanging drop vapor

diffusion method at 20 °C. Equal volumes of GlxA solution at a concentration of 15 mg ml^{-1} and reservoir solution containing 0.1 M sodium acetate pH 4.0, 20% PEG 20,000 were mixed. Crystals suitable for diffraction studies grew within 1 week. A single crystal was transferred to a cryoprotectant solution containing, the respective reservoir solution and 20 % glycerol prior to flash-cooling by plunging into liquid nitrogen. Crystallographic data were measured at the beamline I03, Diamond Light Source, using an X-ray wavelength of 0.979 Å and a Pilatus 6-M-F detector (Dectris). Details of structure determination are given in Supporting Information. Coordinates and structure factors were deposited in the RCSB Protein Data Bank with accession number 4unm. A summary of data and refinement statistics and the quality indicators for the structure are given in Table 1. CAVER analyst 1.0 was used for the identification of tunnels (Kozlikova *et al.*, 2014). Chain B of GlxA was analysed using the tunnel computation tool within CAVER with a starting point defined using the first coordination sphere Cu binding residues (Tyr^{289}, Tyr^{501}, His^{502}, His^{589}). Default settings for tunnel analysis were used, including the minimum probe radius set to 0.9 Å.

Table 1. *X-ray data processing and refinement parameters. The GlxA crystal structure was in space group $P2_1$ with unit cell parameters 50.4, 126.6, 107.6 Å, 90, 91.1, 90º. Values in parentheses refer to the outermost resolution shell (1.80-1.77 Å).*

Resolution (Å)	53.3-1.77
Unique reflections	130533 (21898)
Completeness (%)	99.7 (99.6)
Redundancy	3.6 (3.4)
Rmerge (%)	0.064 (0.633)
Mn(I/sd)	10.5 (2.0)
Wilson B factor (Å2)	20.5
Rcryst	0.188
Rfree	0.228
RMSD bond lengths (Å)	0.011
RMSD bond angles (º)	1.41
ESU based on ML (Å)	0.096
Ramachandran favoured (%)	95.9
PDB accession code	4unm

EPR spectroscopy

GlxA samples (85-120 µM) for EPR were prepared in duplicate in a mixed buffer system consisting of 10 mM each of Tris, potassium acetate, MES, MOPS and 200 mM KCl with the pH adjusted to 7.0. Wilmad SQ EPR tubes (Wilmad Glass, Buena, NJ) were filled with the GlxA solutions and frozen in methanol kept on dry ice. The tubes were then transferred to liquid nitrogen. All EPR spectra were measured on a Bruker EMX EPR spectrometer (X band) at a modulation frequency of 100 kHz. A spherical high-quality Bruker resonator

ER 122 SP 9703 and an Oxford Instruments liquid helium system were used to measure the low-temperature EPR spectra. Digitising of a published EPR spectrum was performed using Un-Scan-It, v.6, Silk Scientific.

Activity assays

A variety of putative substrates for GlxA were assayed. These included the following monosaccharides; D-galactose, D-glucose, D-sucrose, D-fructose *N*-acetyl-D-glucosamine, and D-glucuronic acid; the disaccharides, D-lactose and D-cellobiose; and the aldehydes and primary alcohols glycolaldehyde, glyoxal and glycerol (all purchased from Sigma). Catalytic turnover was measured using a coupled assay, whereby the production of H_2O_2 by GlxA was detected by the presence of horseradish peroxidase (HRP) (Sigma) and the subsequent oxidation of guaiacol (Sigma). Samples were prepared in 3 ml quartz cuvettes containing 0.1 M sodium phosphate, pH 7.4, 1 mM guaiacol, 1 µl HRP (10 mg ml^{-1}), 20-30 µM GlxA and varying concentrations of the individual substrate. The oxidation of guaiacol was monitored at 470 nm using a Hewlett-Packard 8453 diode-array spectrophotometer scanning between 190 and 1100 nm and thermostatted at 25 °C. Plots of turnover rate (k, s^{-1}) versus substrate concentration were constructed, whereby k was calculated from $((\Delta A_{470}/\varepsilon_{gc})/t)/[GlxA])$ where ΔA_{470} is the absorbance change at 470 nm upon guaiacol oxidation, ε_{gc} is the extinction coefficient of the guaiacol oxidation product taken as 5.57 mM^{-1} cm^{-1}, t is the time in seconds and [GlxA] is the total millimolar concentration of GlxA in the assay.

Results

GlxA is associated with the membrane

The distribution of GlxA in the soluble and insoluble fractions of liquid grown *S. lividans* mycelium was first determined. Upon thorough mycelium sonication followed by centrifugation steps, a small fraction of GlxA was detected in the soluble protein fraction (S100) with the majority remaining in the pellet fraction (P30 and P100) (Fig. 1A and B). In contrast, the majority of the cytoplasmic marker EF-Tu1 is detected in the soluble fraction (S100) (Fig. 1A and B). Resuspension of the insoluble pellet fraction in buffer containing 1 % Triton X-100 solubilizes a significant amount of GlxA (Fig. 1A and B), indicating that GlxA is not covalently bound to the membrane. However, salt washes did not remove GlxA from intact mycelium (Fig. 1C), but small amounts of EF-Tu1 were detected probably due to some lysis. These data show that GlxA is not a peripheral membrane protein but is firmly associated with the membrane, although not via a covalent bond. These results are in agreement with *in silico* analysis, which predict residues 1-11 of GlxA to be an N-terminal signal peptide (Petersen *et al.*, 2011), with a weak signal peptidase cleavage site between

residues 11-12, followed by a transmembrane helix (residues 12-32), which could function as the membrane anchor (Käll *et al.*, 2004; Bagos *et al.*, 2008).

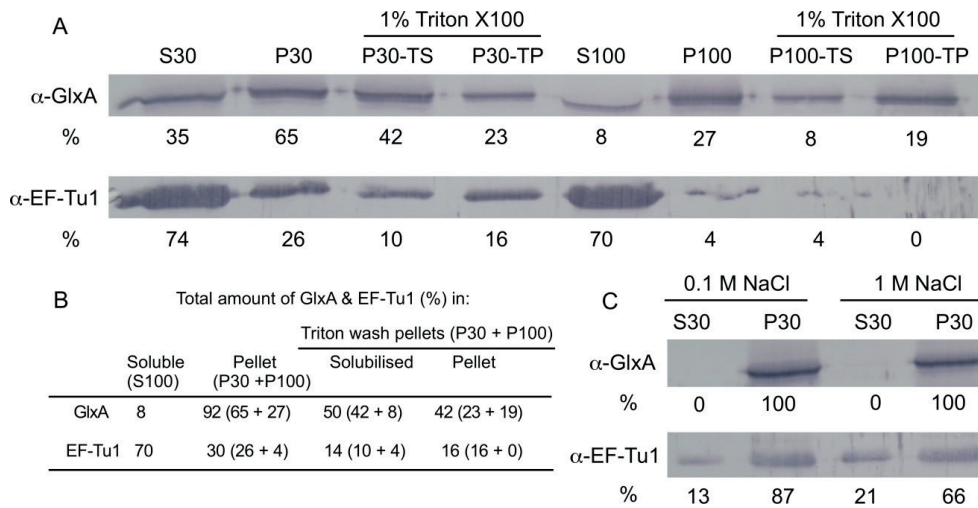

Figure 1. *Location of GlxA in the mycelium determined by Western blotting.* ***A)*** *Detection of GlxA and EF-Tu1 in the various mycelium fractions. Samples were prepared as described in "Experimental". The band intensities are expressed as percentages relative to the total amount of GlxA or EF-Tu1 in the S30 plus P30 fraction, of which the intensity was set at 100%.* ***B)*** *The Table presents the total soluble (S100), 1% triton soluble (P30-TS + P100-TS) and insoluble fraction (P30-TP + P100-TP) of GlxA and EF-Tu1 expressed in percentage according to (A).* ***C)*** *NaCl washes of the intact mycelium. The signals detected in the S30 plus P30 samples of the 100 mM NaCl wash was set at 100%.*

The tertiary structure of GlxA consists of three distinct domains

To elucidate the molecular features of GlxA, an N-terminal truncated expression construct (Δ1-34) for over-expression in *E. coli* was generated, which yielded 45 $mg \cdot L^{-1}$ of purified GlxA. The crystal structure of GlxA was determined to 1.77 Å resolution and contains two protein molecules in the crystallographic asymmetric unit. Molecule A (residues 38-645) exhibits significantly lower B-factors and higher quality electron density than molecule B, but contains a disordered region between residues 198-206 (not visible in the electron density), whereas the main chain for molecule B was complete between residues 37 and 645. The overall structure of GlxA (Fig. 2) consists of three predominately β-sheet domains. Preceding the first domain are two short N-terminal α-helices (α1 and α2), with the α1 helix orientated approximately perpendicular to the α2 helix. Domain 1 of GlxA consists of seven Kelch motifs (blades) arranged in a β-propeller tertiary structure (Fig. 2). Each blade of the propeller consists of four anti-parallel β-sheets (*a*, *b*, *c*, *d*) with each sheet connected through variable length loops (Fig. 2). Blades 1 and 2 each possess structural inserts in the loops connecting sheet *b* to sheet *c*. In blade 1 a short platform-like α-helix (α3) is inserted which has an overall negative charge, whereas in blade 2, sheets *b* and *c* are connected via domain 2 (Fig. 2). Domain 2 consists of 10 β-sheets and 1 short α-helix (α4). According to the CATH

database (Sillitoe *et al.*, 2013) the domain 2 fold is classified as mainly β, with a β-barrel architecture formed by sheets 1, 3, 4, 8, 9 and 10 (Fig. 2), and a representative domain topology with thrombin, subunit H. Protruding out from the core β-barrel is a long β-hairpin loop (residues 194-210) consisting of β-sheets 6 and 7 (Fig. 2). In molecule A this β-hairpin loop is disordered and not built into the model, whereas this is not the case for molecule B due to stabilising polar interactions with molecule A residues from a symmetry related GlxA molecule in the unit cell (Supplementary Fig. S2). Domain 2 is positioned in the overall tertiary structure such that the β-barrel core lies across the top of approximately half of domain 1 with the β-hairpin loop extending into the solvent (Fig. 2). Further analysis of domain 2 using PDBeFold identifies no structures deposited in the PDB with a high structural homology (the highest Q-score obtained was only 0.14). Thus the fold of domain 2 in GlxA is relatively novel compared to known structures. The third domain starts immediately after the seventh Kelch motif and is located at the bottom of domain 1. Domain 3 consists of

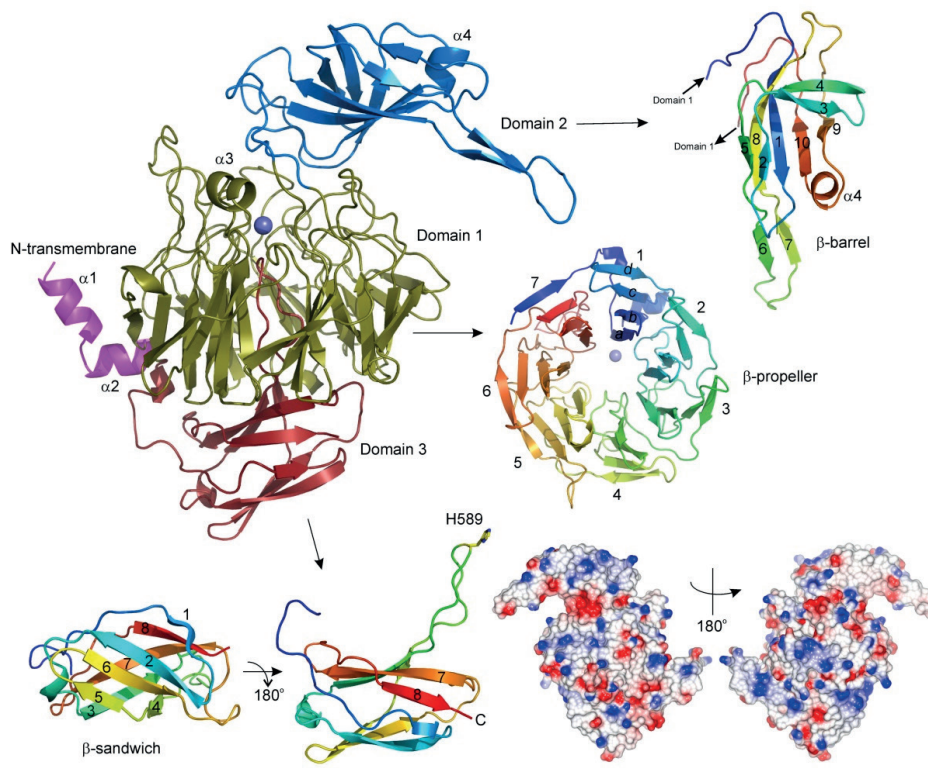

Figure 2. *X-ray crystal structure of S. lividans GlxA. The three domains forming the tertiary structure are indicated and coloured gold (domain 1), blue (domain 2) and red (domain 3). The four short α-helices present in the structure are labelled. Each domain is shown individually and in more detail as discussed in the main text. The Cu atom is represented as a sphere and electrostatic surface representations in two GlxA orientations are shown. Images were prepared in PyMol and CCP4MG (McNicholas et al., 2011).*

8 β-sheets and one short α-helix forming a β-sandwich fold with a high structural homology to domain 3 of Gox (1.18 Å RMSD from superimposition). A loop (residues 583-590 in GlxA) connecting β-sheets 3 and 4 of domain 3 penetrates upwards into domain 1 along the 7-fold symmetry axis and provides one of the ligands (His^{589}) to the Cu ion of GlxA (*vide infra*). The charge distribution of GlxA (pI 8.2) is displayed through electrostatic surface representations (Fig. 2), and indicates a rather disperse distribution of charge across the whole molecular surface.

Architecture and spectroscopic properties of the Cu site in GlxA

A well-defined 16σ peak in the σ-weighted F_o-F_c difference map was present in each GlxA chains in the asymmetric unit, into which a Cu ion was modelled. The Cu is coordinated in a square pyramidal geometry with the Oγ of Tyr^{501} acting as the axial ligand and the equatorial coordination positions occupied by the Oγ of Tyr^{289}, the Nε2 of His^{502} and His589 and a H_2O molecule (Fig. 3A). Bond lengths to the Cu ion are reported in Table 2 together with a comparison to those in Gox. Unbroken electron density is observed between the side chain Sγ atom of Cys^{121} and the Cε1 ring atom of Tyr^{289}, providing clear evidence that a cross-linked Tyr-Cys cofactor is formed in GlxA, with a bond length of 1.9 Å (2.0 Å in chain B) (Fig. 3A). Adjacent to Tyr^{289} is Trp^{288}, which has its side chain indole ring orientated such that the benzene ring is π-π stacking with the phenoxyl ring of Tyr^{289} with C^{Tyr}-C^{Trp} distances between ~ 3.5 and 4 Å (Fig. 3A).

The UV-Vis absorbance spectrum of the blue-grey Cu(II)-GlxA has a broad, low intensity band in the visible region (λ_{max} ~ 577 nm) and two distinct shoulders (λ_{max} ~ 362 and 320 nm) (Fig. 3B). No change to these absorption features in the pH range 4 to 8 was observed, with the addition of Cu(II) ions resulting in only a small absorbance increase in λ_{max} ~ 577 nm over a 12 h period (Fig. 3B). In contrast the Cu(II)-Gox absorption spectrum has weak intensity bands at λ_{max} 441 nm attributed to phenolate (Tyr) to Cu(II) ligand-to-metal charge transfer (LMCT) and at λ_{max} 630 nm arising from mixed Cu ligand field transition and LMCT (Whittaker and Whittaker, 1988; Whittaker and Whittaker, 1993). Addition of the reductant $Na_2S_2O_4$ bleaches all absorption features (Fig. 3B) with removal of $Na_2S_2O_4$ and subsequent exposure to air resulting in the return of the Cu(II)-GlxA spectrum. This infers that the Cu is redox active and can cycle between the Cu(II) and Cu(I) states.

The EPR spectrum of Cu(II)-GlxA at pH 7 displays features consistent with an axial Cu(II) g-tensor, $g_{||}$ = 2.182 and $g_{\perp}$ = 2.05 (Fig. 3C). The strong line on the right from the indicated $g_{\perp}$ region is not a principal g-factor component but an “overshoot” line (Antholine, 2005) occurring for specific orientations of the Cu(II) complexes, subject to particular relationships between the values of $g_{||}$, $g_{\perp}$ and the anisotropic components of the hyperfine interaction of the electron spin (S = 1/2) with the Cu nuclear spin (S = 3/2), $A_{||}$ and $A_{\perp}$. The EPR spectrum

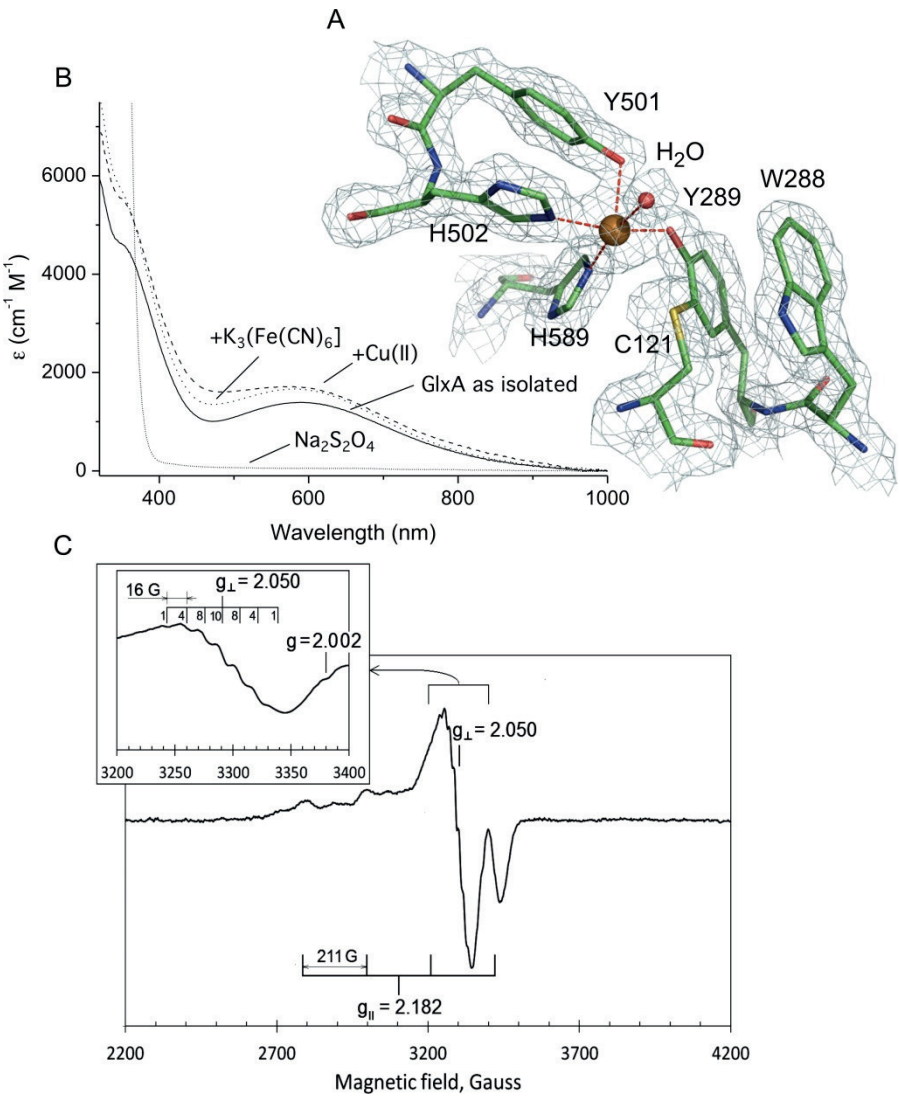

Figure 3. *Structure and spectroscopy of the GlxA Cu site.* ***A)*** *$2F_o$-F_c electron-density map contoured at 2σ of the Cu site in GlxA. The Cu ion is represented as a brown sphere with the first coordination sphere ligands to the Cu ion depicted as sticks and the equatorially coordinating H_2O molecule as a red sphere.* ***B)*** *Absorbance spectrum at pH 7 and 20 °C of purified GlxA (80 μM) and following the addition and removal of the oxidant $[Fe(CN)_6]^{3-}$, the reductant $Na_2S_2O_4$ and Cu(II)SO_4.* ***C)*** *Cu(II)-GlxA EPR spectrum (85 μM) at pH 7. The $g_{//}$ component shows a hyperfine interaction of the electron spin (S = 1/2) with the I = 3/2 Cu nuclear spin – four components 1:1:1:1 separated by A_z^{Cu} = 211 G. Inset: the $g_\perp$ region of the spectrum, which displays unpaired electron (S = 1/2) hyperfine interaction of the electron spin with the Cu(II) ligands – seven components of relative intensities 1:4:8:10:8:4:1 separated by 16 G. Instrumental conditions: temperature 10 K, microwave frequency ν_{MW} = 9.47 GHz, microwave power P = 3.18 mW, modulation frequency ν_M = 100 kHz, modulation amplitude A_M = 5 G, time constant τ = 82 ms, scan rate V = 22.6 G·s^{-1}, number of scans per spectrum NS = 1.*

Table 2. *Bond lengths of the Cu sites (monomer A and B) in S. lividans GlxA and F. graminearum Gox (PDB 1gof) (Ito et al., 1994).*

GlxA (A/B)		Gox	
Cu-Tyr289 OH	1.84/1.97 Å	Cu-Tyr272 OH	1.93 Å
Cu-Tyr501 OH	2.24/2.14 Å	Cu-Tyr495 OH	2.69 Å
Cu-His502 Nε2	2.13/2.18 Å	Cu-His496 Nε2	2.11 Å
Cu-His589 Nε2	2.18/2.23 Å	Cu-His581 Nε2	2.14 Å
Cu-H2O	2.44/2.50 Å	*Cu-acetate	*2.26 Å
Tyr289-Cys121	1.92/1.97 Å	Tyr-Cys	1.83 Å

**1gof crystallised in acetate buffer pH 4.5 (GlxA acetate buffer pH 4.0), with an acetate molecule found in place of the H_2O molecule in GlxA. In a Gox structure (1gog) (Ito et al., 1991) crystallised in the absence of acetate buffer at pH 7.0 a H_2O molecule is found with a bond length to the Cu ion of 2.81 Å.*

line shape is similar to that of Cu(II)-Gox (Whittaker and Whittaker, 2003), which also has an axial Cu(II) g-tensor (Peisach and Blumberg, 1974; Cleveland *et al.*, 1975; Bereman and Kosman, 1977). However, the GlxA spectrum exhibits a more distinctly resolved overshoot line, likely to be a consequence of a smaller $g_{||}$ (2.182 as compared to 2.21-2.23 in Gox). The $g_{\perp}$ component displays a hyperfine interaction of the electron spin with the Cu(II) ligands, which for GlxA gives seven lines with relative intensities of 1:4:8:10:8:4:1 (Fig. 3C, inset) compared to five lines in Gox (Cleveland *et al.*, 1975; Bereman and Kosman, 1977).

Substrate access sites and binding pocket

Due to the buried nature of the Cu site, it is likely that a substrate would have to gain access via a tunnel. CAVER was used to identify tunnels in the GlxA structure (Chovancova *et al.*, 2012; Kozlikova *et al.*, 2014), defined as void pathways leading from a cavity inside GlxA, *i.e.* the Cu site, that transverse to the protein surface. Three tunnels of different lengths were identified (Fig. 4A). The entrance to tunnel I lies between the α3 helix on the loop connecting sheets *a* and *b* in blade 1 and a well-ordered loop in blade 7 of domain 1 (Fig. 4A and B). The tunnel has an opening of ~ 8 x 8 Å, is void of H_2O molecules and leads directly to the equatorially Cu coordinating H_2O molecule, with a distance to the surface of ~ 10 Å. The dimensions of the surface opening are such that pyranose carbohydrates e.g. D-glucose or D-galactose, and also C2 substituted pyranose carbohydrates such as *N*-acetyl-glucosamine would be able to pass. The opening of tunnel II is located beneath the β-hairpin loop of domain 2 (Fig. 4B), with the dimensions of the opening, ~ 9 x 7 Å. A network of six H-bonded H_2O molecules are present in the tunnel that thread down to the Cu coordinating H_2O molecule, with a distance to the surface of ~ 25 Å. Tunnel III spans a large section of domain 1, starting from below the equatorial His ligands and leading to a surface entrance formed by residues Ala^{128}, Gly^{298}, Pro^{322} and Ser^{622}. The tunnel is lined with a continuous network of well-ordered H_2O molecules (13 in total) and has a distance from the Cu ion to the surface

of ~ 70 Å. A putative substrate pocket is identified above the axial Tyr^{501} ligand and is directly accessible from either tunnel I or II (Fig. 4C). The pocket is occupied with several H_2O molecules, all of which are well ordered and form an extensive H-bond network, which also includes a H-bond interaction with the Tyr^{501} ligand (Fig. 4C). The pocket is completely polar and is formed from the side chains of 6 amino acids (Fig. 4C). Side-chain H-bonding interactions with the H_2O network in the pocket are apparent for some of the residues (Fig. 4C), with Asn^{88} and Arg^{469}, part of the entrance to tunnel I (Fig. 4B), also capable of

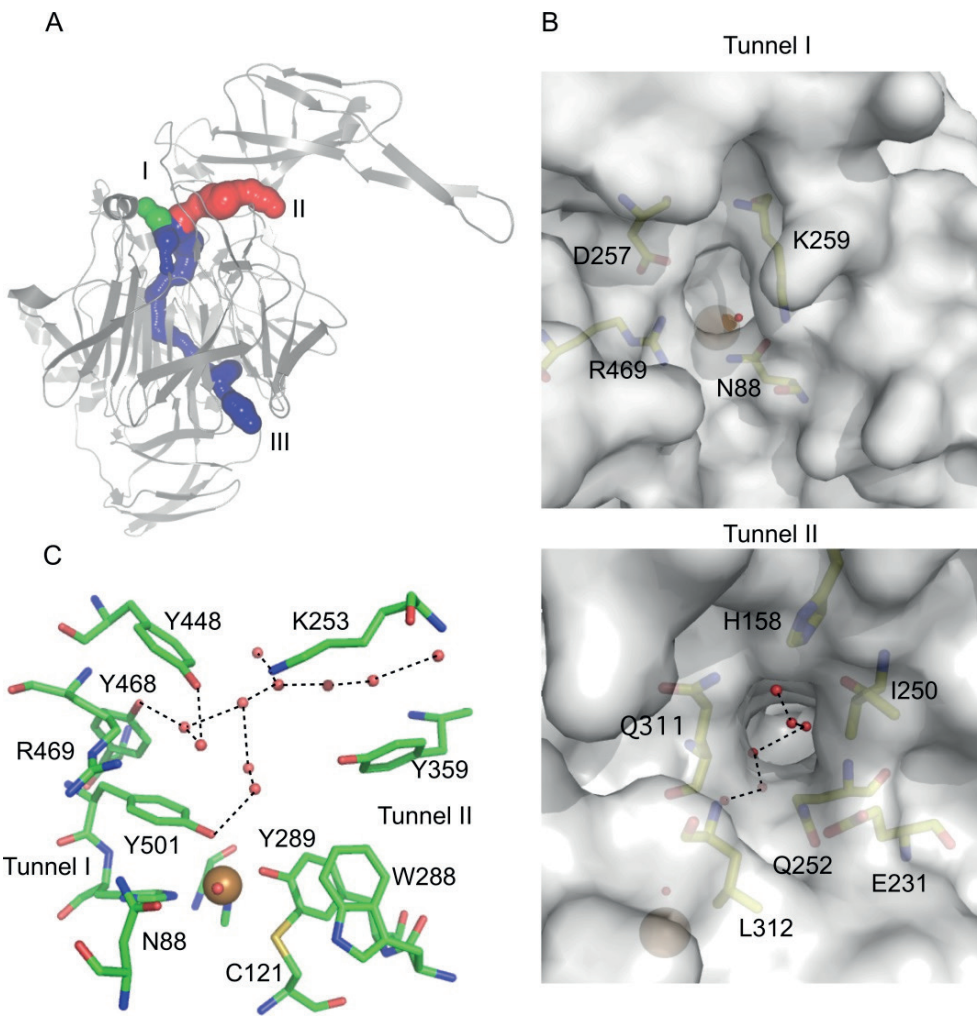

Figure 4. *Substrate access channels and binding pocket.* ***A)*** *Location of the three surface-to-Cu site tunnels (I, II, III) in S. lividans GlxA identified using the programme CAVER (Kozlikova et al., 2014).* ***B)*** *Partial transparent surface views of the openings to tunnels I and II. The amino acids forming the openings are labelled and shown as sticks, H_2O molecules are depicted as red spheres and the Cu ion as a brown sphere. In tunnel I the equatorially Cu co-ordinated H_2O molecule is visible, and tunnel II illustrates the H-bonded H_2O network leading from the surface to the Cu site.* ***C)*** *The putative substrate-binding pocket in GlxA.*

H-bond interactions.

The Tyr-Cys crosslink is redox active

The Tyr-Cys cross-link identified in the GlxA X-ray structure is redox active in Gox. Addition of the oxidants, $[Fe(CN)_6]^{3-}$ or $[Ir(Cl)_6]^{3-}$, to Cu(II)-GlxA does not perturb the absorbance spectrum (Fig. 3B) in contrast to Gox where formation of the fully oxidised Cu(II)-Tyr-Cys• form leads to distinct spectral features. However, a change in the EPR spectrum of GlxA following addition of $[Fe(CN)_6]^{3-}$ is observed, with a 3 component free radical EPR spectrum detected (Fig. 5). The spectrum is very similar to the spectrum of the radical on the Tyr-Cys crosslink reported for Gox (Whittaker and Whittaker, 1990), glyoxal oxidase (Whittaker *et al.*, 1999) and SCO2837p from *S. coelicolor* (Whittaker and Whittaker, 2006) (Fig. 5). This observation taken together with the result of $Na_2S_2O_4$ reduction indicates that the active site of GlxA can access three oxidation states (reduced (Cu(I)), semi-reduced (Cu(II)) and fully oxidised (Cu(II)-Tyr-Cys•) as is the case for Gox and should therefore be able to catalyse the two-electron oxidation of a substrate.

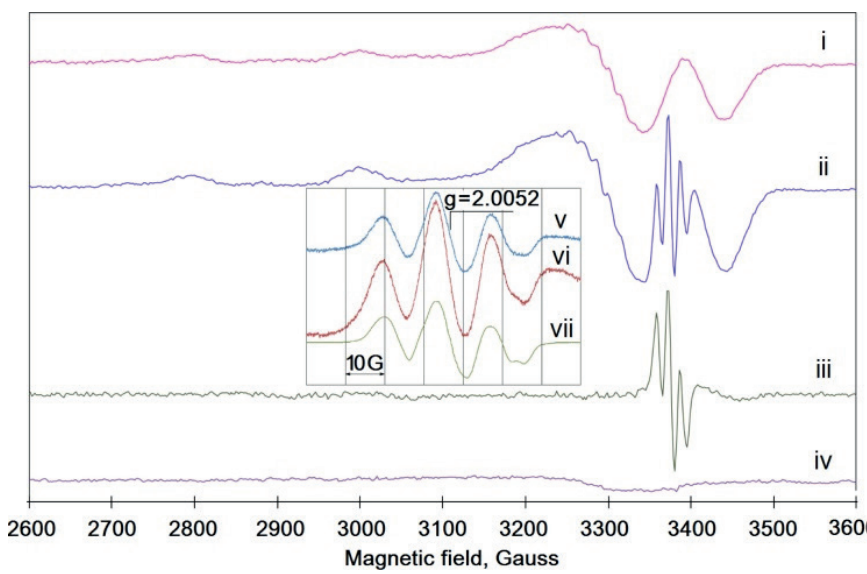

Figure 5. *EPR spectra of Tyr-Cys radicals.* ***i)*** *As isolated GlxA.* ***ii)*** *After $[Fe(CN)_6]^{3-}$ treatment.* ***iii)*** *difference spectrum (ii-1.46 x i) showing the free radical EPR signal in its pure form (the coefficient 1.46 was found empirically to minimize input of other EPR signals to the difference spectrum).* ***iv)*** *As in (i), but after $Na_2S_2O_4$ treatment.* ***Inset:*** *the same sample as the one used to detect spectrum (ii), was used to measure the free radical EPR signal in greater detail using two different microwave power levels, 50 µW* ***(v)*** *and 3.18 mW* ***(vi)****.* ***vii)*** *The EPR spectrum of the radical in SCO2837p from S. coelicolor (Whittaker and Whittaker, 2006). All spectra were recorded at 40 K using 120 µM of GlxA at pH 7, with the instrumental conditions for i, ii and iv the same as in Fig. 3C and for spectra v and vi as follows: modulation amplitude A_M = 3 G, scan rate V = 0.596 G s^{-1}. Spectrum vii is a digitised image from (Whittaker and Whittaker, 2006), aligned with the GlxA spectrum on the basis of g-factors, therefore the magnetic field axis is not indicated.*

Enzymatic activity of GlxA

A number of compounds were assayed for activity with GlxA using a coupled peroxidase assay (see "Experimental"), with only four showing significant oxidase activity. Fig. 6A reveals that aerobic oxidation rates for D-galactose, D-glucose and glycerol, follow a linear substrate relationship for the concentrations used. From the slopes of these plots, second order rate constants (k_{red}) were determined for D-galactose; 8.4 x 10^{-3} $M^{-1}s^{-1}$, for D-glucose; 8.8 x 10^{-3} $M^{-1}s^{-1}$ and for glycerol; 1.7 x 10^{-2} $M^{-1}s^{-1}$. No activity was observed for the C2 position modified monosaccharide *N*-acetyl-D-glucosamine or for fructose, a 5-membered ring monosaccharide. Likewise D-glucuronic acid gave no activity, illustrating that a C1 glycosidic (aldehyde) group is not effective as reductant when the C6 group is modified (COOH *vs* CH_2OH). Furthermore, no activity was detected with the disaccharides D-lactose and D-cellobiose. In addition to catalysing the oxidation of primary alcohols, Gox has been reported to convert aldehydes to the corresponding carboxylates (Kelleher and Bhavanandan, 1986). However, the aldehyde, glyoxal, turned over by glyoxal oxidase, also did not give activity with GlxA. In contrast, glycolaldehyde ($C_2H_4O_2$) the smallest molecule to contain both an aldehyde and a hydroxyl group gave significant activity with GlxA that followed Michaelis-Menten kinetics (Fig. 6B). From these data a K_m for glycolaldehyde of 115 mM and a maximal aerobic turnover (k_{cat}) of 0.14 s^{-1} was determined. The corresponding k_{cat}/K_m value of 1.22 M^{-1} s^{-1} enables a direct comparison with the two monosaccharides and glycerol, with glycolaldehyde reacting 100-times faster.

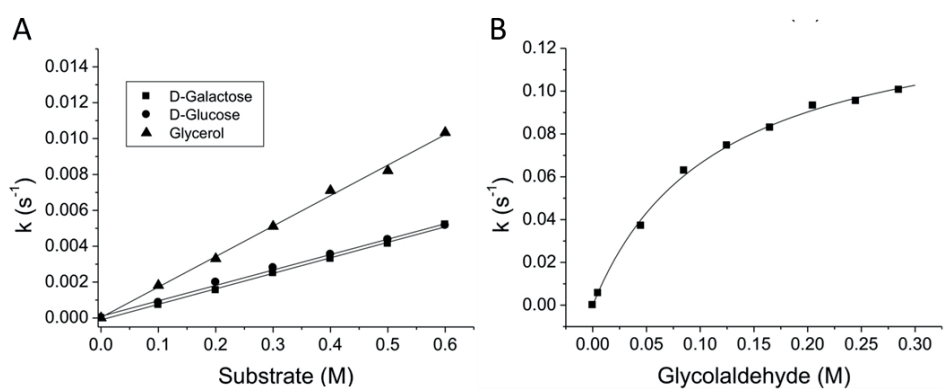

Figure 6. *Enzyme activity of S. lividans GlxA.* ***A and B)*** *Plots of turnover rates (k) for GlxA with four different substrates (25 °C). In (A) the line of best fit through the data points enables a second-order rate constant (M^1s^1) to be determined. In (B) the data points have been fitted to the Michaelis-Menten equation to yield a K_m value and turnover (k_{cat}) reported in the main text.*

GlxA is required for glycan synthesis at hyphal tips and morphogenesis

To investigate a functional role of GlxA, we created a null-mutant in *S. lividans*. Consistent

with previous work in *S. coelicolor*, our *S. lividans glxA* null-mutant has a bald phenotype (*i.e.* no aerial hyphae formation) on solid media, as is also the case for the *cslA* null-mutant (Xu *et al.*, 2008; Liman *et al.*, 2013) (Fig. 7A). Notably, the bald phenotype in the *glxA* and *cslA* null-mutants cannot be rescued upon addition to the medium of exogenous Cu(II) (Fig. S3) as has previously been reported for the Δ*sco* null-mutant (Blundell *et al.*, 2013). Furthermore, the *glxA* and *cslA* mutants have an identical morphology in liquid-grown

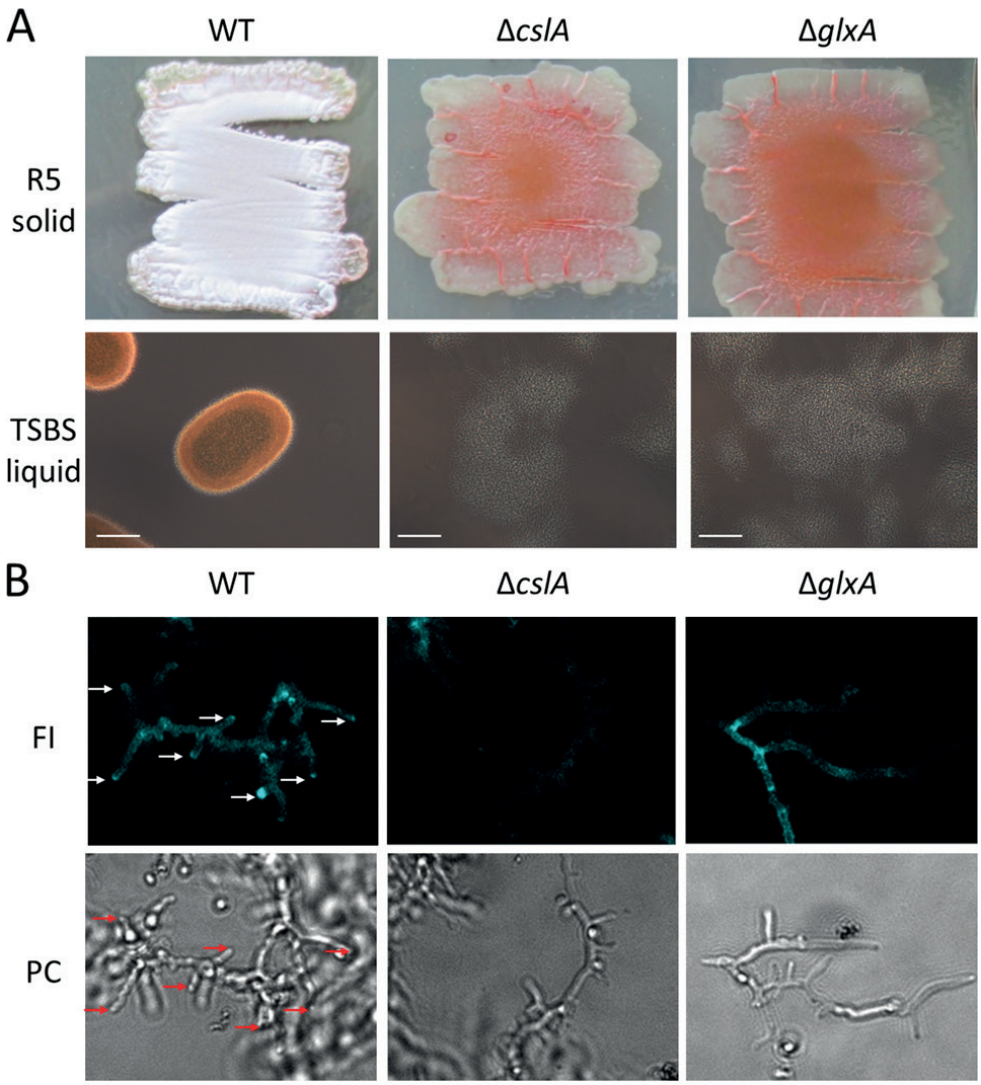

Figure 7. *Deletion of cslA or glxA in S. lividans leads to a block in development and abolishes pellet formation and glycan deposition.* ***A)*** *Growth on solid R5 medium and pellet formation and dispersed growth in TSBS 24 h liquid cultures. Scale-bar (white line) is 100 µm.* ***B)*** *CFW staining in 24 h mNMMP standing cultures shown in fluorescence image (FI) and phase contrast brightfield (PC). Arrows indicate tip staining that is present in WT cultures but not in mutants.*

cultures. Instead of the dense compact pellets seen in WT, the mutants grow with an open mycelium phenotype (van Dissel *et al.*, 2014) (Fig. 7B). The transcriptomes of the *glxA* and the *cslA* mutant as analysed by RNA-seq revealed increased expression of genes related to osmoprotection indicating that the mutants suffer from osmotic stress (data not shown) and is in agreement with the observation of Liman et al. (2013). Excitingly, mycelial staining with calcofluor white (CFW), which binds to β-(1-4) glycans indicated that the hyphal tips in both the *cslA* and *glxA* null mutants were no longer stained, in contrast to those of the WT strain (Fig. 7B). This indicates that in addition to CslA, GlxA is required for glycan synthesis or attachment to hyphal tips.

Discussion

Results from the present study reveal that *S. lividans* GlxA is a membrane-associated cuproenzyme required for the production or localisation of the hyphal tip glycan. The spectroscopic properties, tertiary structure and enzymatic profile are all distinctly different to its fungal counterpart Gox, thus making GlxA a new structural and functional member of the mononuclear Cu oxidase family.

From a spectroscopic perspective a number of features in GlxA stand out. In the Cu(II)-GlxA EPR spectrum, the $g_{\perp}$ component displays a hyperfine interaction of the electron spin with the Cu(II) ligands, giving rise to 7 lines with relative intensities 1:4:8:10:8:4:1 yielding a 16 G splitting (Fig. 3C inset). For Cu(II)-Gox, a quintet line structure of relative intensities 1:2:3:2:1 (Cleveland *et al.*, 1975; Bereman and Kosman, 1977) and a distance between the lines typical for a N hyperfine interaction (14-18 G) (Berliner *et al.*, 2001; Kirima *et al.*, 2003) consistent with two His ligands is observed. The source of the additional hyperfine splitting in GlxA is presently unclear and requires further investigation, but would suggest that differences in the electronic properties of the Cu(II) site in GlxA and Gox exist. A further anomaly in the spectroscopic properties between GlxA and Gox is in relation to the spectral observation of the Tyr-Cys• radical. EPR spectroscopy clearly indicates the presence of this radical (Fig. 5) following addition of an oxidant to Cu(II)-GlxA. However, no perturbation of the Cu(II)-GlxA absorbance spectrum is observed as is the case on forming Cu(II)-Tyr-Cys• in Gox. Furthermore, the Cu(II)-GlxA optical spectrum does not resemble that of Cu(II)-Gox (Whittaker and Whittaker, 1988). The coordination geometry of the Cu(II) site in both GlxA and Gox are identical, but as indicated by EPR could be electronically distinct and the possibility of second sphere coordination effects having an effect could be possible. In this respect the most pertinent difference between GlxA and Gox is in the side chain orientation of Trp^{288} (Trp^{290} in Gox). In Gox, Trp^{290} has been proposed to provide an extended aromatic system with its indole ring stacking over the Tyr-Cys bond, stabilising the delocalisation of the radical (Fig. 8D) (Ito *et al.*, 1991; Rogers *et al.*, 2007). However, in GlxA Trp^{288} no longer has its indole ring stacking with the Tyr-Cys cross-link, but instead has the benzene ring

component π-π stacking with the Tyr[289] Cu ligand (Fig. 8D). In combination with a more insulated (buried) Cu site, the re-orientation of the Trp side chain may influence the electronic transitions of the Cu and the radical and result in the markedly different absorbance spectrum for GlxA compared to Gox.

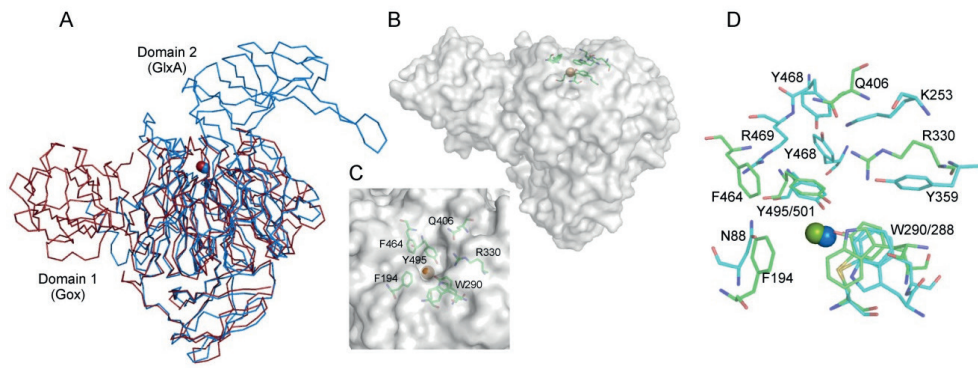

Figure 8. *Structural comparison of GlxA with Gox (1gof) (Ito et al., 1991).* ***A)*** *Ribbon representation of a superposition of the Cα atoms of GlxA (blue) with Gox (red). The Cu ions are shown as spheres.* ***B)*** *Surface representation of Gox, with location of the Cu ion (brown sphere) and residues in the substrate pocket indicated in sticks.* ***C)*** *View of the substrate pocket looking down the 7-fold symmetry axis towards domain 3 of Gox. The location of the surface exposed Tyr[495] Cu ligand and the stacking Trp[290] as well as residues forming the substrate pocket are shown in sticks, with the solvent exposed Cu represented as a sphere.* ***D)*** *Superposition of the substrate pockets in GlxA (blue) and Gox (green).*

The ability to generate 3 oxidation states in GlxA suggests an enzymatic function in *S. lividans*. However, none of the substrates tested exhibit activity with GlxA that is comparable to Gox (with the exception of D-glucose). This is exemplified with D-galactose, the canonical monosaccharide substrate for Gox, where under aerobic conditions a k_{cat}/K_m value of 10^{-3} $M^{-1}s^{-1}$ for GlxA is determined, which is a million times lower than for Gox (Baron *et al.*, 1994) and is equivalent to Gox with D-glucose (Sun *et al.*, 2002). The most active substrate tested with GlxA, glycolaldehyde, has a K_m value (115 mM) comparable to Gox for D-galactose (70-80 mM), but a k_{cat}/K_m value > 4-orders of magnitude lower. For Gox the turnover of glycoladehyde has been reported to be 75 % of the D-galactose rate (Arends *et al.*, 2006). These slow turnover kinetics indicate that GlxA has very different substrate specificity compared to Gox with gross structural differences discussed below a likely discriminant.

The distinctness of the GlxA structure can be appreciated from the superposition with Gox in Fig. 8A. In Gox the domain arrangement and surface flatness of the β-propeller domain (domain 2) contributes to a readily accessible Cu site and substrate binding pocket (Fig. 8B and C) (Ito *et al.*, 1991). This is not the case in GlxA, due to the positioning of domain 2 and the longer loop structures of the Kelch motifs. The more accessible nature of the Cu site in Gox is further apparent by the presence of an acetate ion (a buffer component of the

crystallisation solution) coordinating the Cu in the X-ray structure. Despite crystals of GlxA also being grown from acetate buffer, no evidence for an acetate ion, in or close, to the Cu site is observed, highlighting the protection afforded to the Cu site in GlxA. Furthermore, a very different structural arrangement of the substrate pocket in GlxA compared to Gox is apparent (Fig. 8D). On one side of the Gox pocket, the side chains of residues Arg^{330}, Gln^{406} and the Nε1 atom of Trp^{290} are posed to provide H-bonds to the canonical D-galactose substrate, with the opposite side of the pocket formed by the aromatic residues, Phe^{194} and Phe^{464}, creating an asymmetric polar/apolar substrate pocket. For GlxA the residues in the pocket, with the exception of Trp^{288}, differ and are not spatially conserved (Fig. 8D). Furthermore, Trp^{288} in GlxA, has its indole ring 'flipped' relative to Trp^{290} in Gox, making this orientation less favourable from a distance perspective for a substrate H-bond interaction in the pocket (Fig. 8D) (Ito *et al.*, 1994). These differences serve to illustrate that despite the Cu coordination being similar, the substrate pockets between Gox and GlxA contain no conserved features. Therefore substrates displaying high turnover kinetics with Gox are unlikely to be optimally accommodated or positioned in GlxA enabling for similar high turnover rates to be achieved.

The observations from the molecular genetics and CFW staining (Fig. 7) indicate that GlxA is directly involved in the production or localisation of the hyphal tip glycan. Synthesis of this glycan also requires CslA, which is a cellulose synthase-like enzyme encoded by the translationally-coupled gene upstream of *glxA*. This glycan accumulates at apical sites during vegetative growth and is absent in the *cslA* mutant (Xu *et al.*, 2008; de Jong, Wösten, *et al.*, 2009; Petrus and Claessen, 2014), and also in the *glxA* mutant. The molecular identity of this glycan is not yet known, but we propose that GlxA acts to modify it through a two-electron oxidation process. It is tempting to speculate that the orientations of tunnels I and II, both connecting at the Cu site (Fig. 4), could be a key structural feature utilised by GlxA in the oxidation of this glycan. A scenario whereby the nascent glycan produced by CslA is fed down into one of these tunnels, orientated in the substrate pocket, oxidised, and then released through the other tunnel may be envisaged. From a biotechnology perspective the open mycelium structure of the *glxA* and *cslA* null-mutants in liquid-grown cultures is of interest for improvement in the utilization of *S. lividans* as an enzyme production host. It has been shown that a more fragmented and therefore also more open mycelium growth in *Streptomyces* increases enzyme production several fold (van Wezel *et al.*, 2006; van Dissel *et al.*, 2014) and that the absence of other glycans result in a distinct morphology in liquid cultures (van Dissel *et al.*, 2015).

Finally, the inability of the Δ*glxA* phenotype to be rescued by Cu, links GlxA to the Cu dependency of *S. lividans* (Fig. S3) and raises the question of how GlxA acquires Cu. Our previous work has inferred that the Cu chaperone Sco delivers Cu to an aa_3-type CcO and also to an unidentified target, which is required to trigger aerial hyphae growth (Blundell *et*

al., 2013; Blundell *et al.*, 2014). To date no other Sco target except CcO in either eukaryote or prokaryote species has been identified. The possibility therefore arises that the second Sco target in *S. lividans* is GlxA. Further experiments aimed at exploring whether this is the case are planned.

Acknowledgements

We acknowledge the award of a University of Essex Silberrad Scholarschip to Amanda Chaplin and the Society of Biology for support of a summer student, Emma Blundell, who assisted in the early stages of this project. Amanda Chaplin cloned, overexpressed and purified recombinant GlxA, crystallized and solved the X-ray structure and performed all spectroscopic and enzymatic activity measurements. Erik Vijgenboom acknowledges NWO/ACTS for grant 053.80.703 in the ERA-IB framework (EIB.08.013 EPOS). Diamond Light Source for access to beamline I03 (East of England Macromolecular Crystallography BAG, MX7461) and use of the JCSG Quality Control Server is acknowledged.

Supporting Information

Introduction

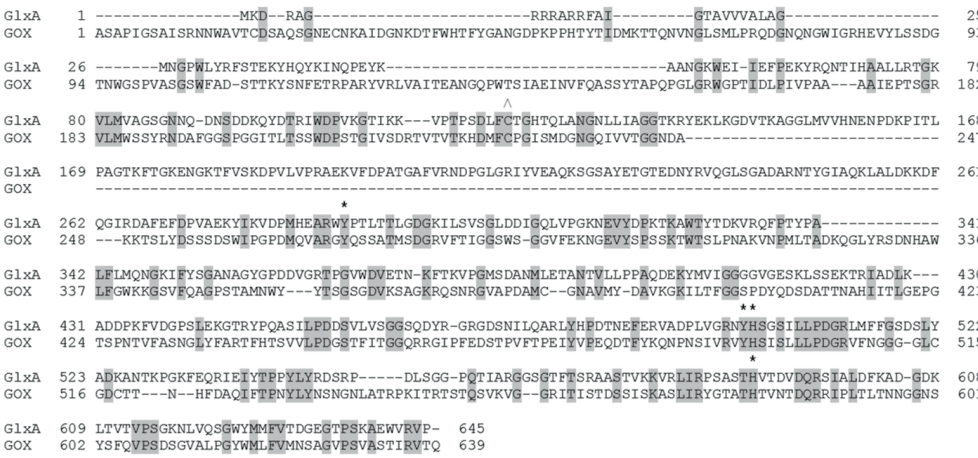

Figure S1. *Clustal omega sequence alignment of Streptomyces lividans GlxA with that of Fusarium graminearum Gox. Sequence conservation is indicated in grey. * indicates sequence position of ligands to the Cu ion and ^ indicates the Cys that forms the Tyr-Cys crosslink.*

Materials and methods

Overexpression and purification of GlxA

GlxA was over-expressed in *E. coli* strain BL21 (DE3) starting from overnight precultures (2 ml 2xYT, 2 µl Kan (50 mg ml^{-1}), 37 °C) that were subsequently used to inoculate 750 ml of medium in 2 L flasks. At an OD600 of 0.6, isopropyl β-D-1-thiogalactopyranoside (IPTG; Melford) was added to a final concentration of 1 mM and the temperature decreased to 25 °C. Cells were harvested after 16 h at 3,501 g and lysed using an EmulsiFlex-C5 cell disrupter (Avestin) followed by centrifugation at 38,724 g for 20 min at 4 °C. The clarified supernatant was loaded to a 5 ml Ni^{2+}-NTA Sepharose column (GE Healthcare) equilibrated with Buffer A (50 mM Tris/HCl, 500 mM NaCl, 20 mM imidazole, pH 8.0) and eluted with a linear imidazole gradient using Buffer B (Buffer A with 500 mM imidazole). A single peak at ~20 % Buffer B was eluted from the column and fractions were pooled and dialysed overnight at 4 °C against Buffer C (50 mM Tris/HCl, 150 mM NaCl, pH 8.0). Following dialysis, the N-terminal His6-tag was removed by incubating the protein at room temperature overnight in the presence of 125 U of thrombin (Sigma). The protein/thrombin mixture was reapplied to the Ni^{2+}-NTA Sepharose column (GE Healthcare) and the flow-through collected and concentrated at 4 °C using a centricon (vivaspin) with a 30 kDa cut-off. Concentrated protein was loaded to a

S200 Superdex column (GE Healthcare) equilibrated with Buffer C and fractions eluting from the major peak (retention volume ~80 ml consistent with a monomer species with a mass in the region of 70 kDa) were concentrated and used in further studies.

Structure determination of GlxA

Diffraction data obtained from GlxA crystals were indexed using iMosflm (Battye *et al.*, 2011) and scaled and merged using Aimless (Evans and Murshudov, 2013) in the CCP4i suite. The structure of GlxA was solved using a model derived from Chainsaw (Stein, 2008), by using the last common atom function and the PDB entry 2eie as the alignment model. Subsequent molecular replacement produced a solution for one of the two molecules in the asymmetric unit that were predicted from the Matthews coefficient. Model building in ARP/WARP (Perrakis *et al.*, 1999) produced a model for one of these GlxA molecules in the asymmetric unit and this was subsequently used as a search model in PhaserMR (McCoy *et al.*, 2007) to locate the second, less well-ordered molecule. Refinement of the structure was carried out using Refmac5 (Murshudov *et al.*, 1997) in the CCP4i suite, with model building between refinement cycles in Coot (Emsley and Cowtan, 2004). Riding hydrogen atoms were added when refinement of the protein atoms had converged. Structures were verified using the Molprobity server (Davis *et al.*, 2007), the JCSG Quality Control Server and Coot (Emsley and Cowtan, 2004).

Results

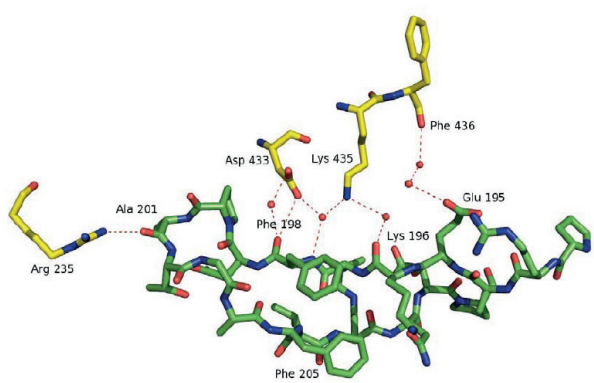

Figure S2. *Stabilizing crystal packing interactions for the β-hairpin loop in chain B of the GlxA structure. Interactions with adjacent molecules are largely solvent-mediated with a small number of direct interactions between amino acids. Note that an additional linkage between the amide nitrogen of Phe^{205} and Lys^{323} of an adjacent molecule, via a bridging water is omitted from the figure for clarity.*

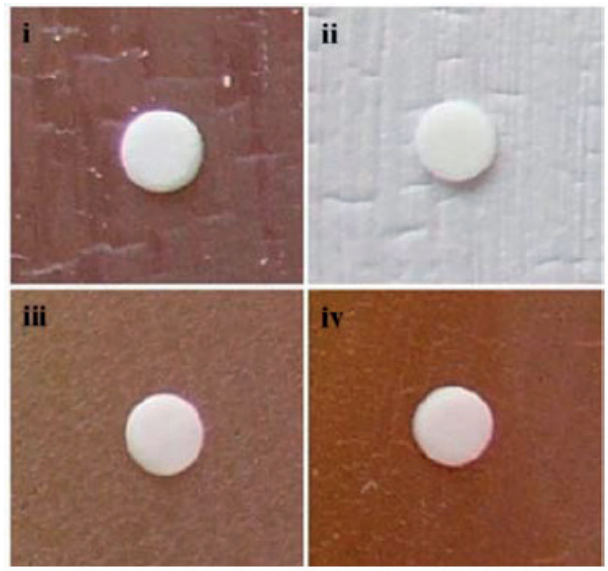

Figure S3. *R5 agar plates were inoculated for confluent growth with S. lividans WT (i and ii) and ΔglxA mutant (iii and iv) spores and incubated for 24 h at 30 °C. No stimulation of development was observed 24 h incubation time after the addition of a Paper filter disk containing 10 µl of 10 mM H_2O_2 on top of the young mycelium (i and iii). The WT showed full uniform development after 96 h (ii) but that development was independent of where H_2O_2 was applied. The mutant did not produce aerial hyphae or spores after 96 h (iv). Therefore H_2O_2 cannot induce development in either the WT or the glxA null-mutant.*

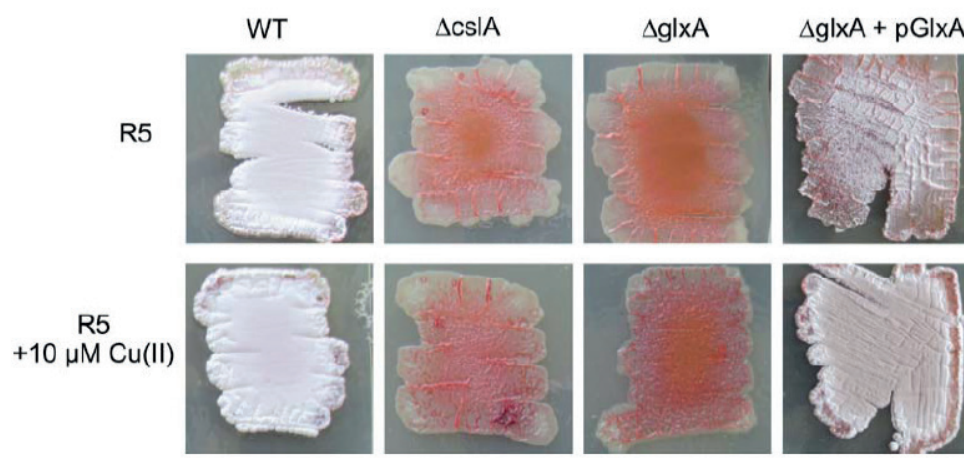

Figure S4. *Complementation of the glxA mutant with a low copy plasmid harboring the glxA gene under control of the cslA promoter results in a wild type morphology on both solid and in liquid media (data not shown). The induction of development by Cu observed in the WT strain is also seen in the complemented glxA mutant.*